THE ASTROPHYSICAL JOURNAL SUPPLEMENT SERIES, 271:20 (10pp), 2024 March https://doi.org/10.3847/1538-4365/ad1c67

A Study of Broad Emission Line and Doppler Factor Estimation for Fermi Blazars

Guohai Chen[1,2,3], Zepeng Zheng[1,2,3], Xiangtao Zeng[1,2,3], Lixia Zhang[1,2,3], Hubing Xiao[4], Xiang Liu[5,6], Lang Cui[5,6], and Junhui Fan[1,2,3]
[1] Center for Astrophysics, Guangzhou University, Guangzhou 510006, People's Republic of China; zhanglixia@e.gzhu.edu.cn, fjh@gzhu.edu.cn
[2] Greater Bay Brand Center of the National Astronomical Data Center, Guangzhou 510006, People's Republic of China
[3] Astronomy Science and Technology Research Laboratory of Department of Education of Guangdong Province, Guangzhou 510006, People's Republic of China
[4] Shanghai Key Lab for Astrophysics, Shanghai Normal University, Shanghai 200234, People's Republic of China
[5] Xinjiang Astronomical Observatory, Chinese Academy of Sciences, Urumqi 830011, People's Republic of China
[6] Key Laboratory of Radio Astronomy, Chinese Academy of Sciences, Urumqi 830011, People's Republic of China
Received 2023 October 18; revised 2023 December 21; accepted 2024 January 3; published 2024 February 26

Abstract

In this work, we obtained a sample of 979 Fermi blazars with broad emission lines, including 701 objects collected from published works and 278 objects developed in this work. For the 278 objects, we made a crossmatch from three catalogs, the Fermi Large Area Telescope Fourth Source Catalog (4FGL), the Sloan Digital Sky Survey, and the Large Sky Area Multi-Object Fiber Spectroscopic Telescope, and calculated the broad-line region (BLR) luminosity. Then, we estimated the Doppler factor and studied the correlations between the BLR luminosities and the γ-ray luminosities, the synchrotron peak frequency (ν_p), and Doppler factor (δ) for the whole sample. Our analyses and discussions came to the following main conclusions: For the 278 blazars, their BLR luminosity (log $L_{\rm BLR}$) ranges from 40.44 to 45.45 erg s^{-1}, with a mean value of 43.39 erg s^{-1}. The Doppler factor ranges from $\delta = 0.45$ to $\delta = 88.52$, with a mean value of 12.99 for the 979 Fermi blazars, which is consistent with the results in the literature. Both the BLR luminosity and the Doppler factor exhibit positive correlations with the γ-ray luminosity. The BLR luminosity is anticorrelated with synchrotron peak frequency, implying a Compton cooling. A line of $\log L_{\rm BLR} = 1.58 \log \nu_p - 19.46$ separating BL Lacertae objects and flat-spectrum radio quasars was obtained in the diagram of $\log L_{\rm BLR}$ against $\log \nu_p$ using a machine-learning method. Based on the analysis of the equivalent width and the Doppler factors, we proposed five changing-look blazar candidates.

Unified Astronomy Thesaurus concepts: Blazars (164); Active galactic nuclei (16); High energy astrophysics (739); Jets (870)

Supporting material: machine-readable tables

1. Introduction

Active galactic nuclei (AGNs), the interesting extragalactic sources, have attracted many astronomers. Blazars are an extreme subclass of AGNs that show many special properties, such as rapid and high-amplitude variability, high and variable polarization, apparent superluminal motion, etc. (Moore & Stockman 1981; Wills et al. 1992; Fan et al. 1997; Romero et al. 2000; Aller et al. 2003; Andruchow et al. 2005; Xie et al. 2005; Abdo et al. 2010; Zheng & Zhang 2011; Zheng et al. 2014; Fan et al. 2016, 2021; Yang et al. 2022b; Xiao et al. 2022d). It is believed that these extreme observational properties are due to a narrow angle between the relativistic jet and the observer's line of sight. In the relativistic beaming model (Padovani & Urry 1990; Urry & Padovani 1995), the beaming factor (or Doppler factor) of the jet is defined by $\delta = [\Gamma(1 - \beta \cos\theta)]^{-1}$, where $\Gamma = (1 - \beta^2)^{-1/2}$ is the bulk Lorentz factor, β is the velocity in units of the speed of light, and θ is the viewing angle. Blazars are divided into two subclasses: BL Lacertae objects (BL Lacs) and flat-spectrum radio quasars (FSRQs). One classical division between BL Lacs and FSRQs is mainly based on the equivalent width (EW) of emission lines; blazars with EW < 5 Å are classified as BL Lacs, while those with EW $\geqslant$ 5 Å are classified as FSRQs (Urry & Padovani 1995). The spectral energy distribution (SED) is also used to classify blazars (Abdo et al. 2010; Fan et al. 2016; Yang et al. 2022a, 2023). Nieppola et al. (2006) divided BL Lacs into low synchrotron peak BL Lacs (LBLs), intermediate synchrotron peak BL Lacs (IBLs), and high synchrotron peak BL Lacs (HBLs). Recently, Fan et al. (2016) calculated SEDs for a sample of 1492 Fermi Large Area Telescope (LAT) blazars, adopted a Bayesian method for the distribution of the logarithm of the synchrotron peak frequencies (logν_p), and proposed classifications using the acronyms defined in Abdo et al. (2010): low synchrotron peak sources (LSPs, $\log(\nu_p/{\rm Hz}) \leqslant 14.0$), intermediate synchrotron peak sources (ISPs, 14.0 <$\log(\nu_p/{\rm Hz})$ 15.3), and high synchrotron peak sources (HSPs, $\log(\nu_p/{\rm Hz})$ >15.3). Yang et al. (2022a) performed similar work for a sample of 2709 Fermi blazars and proposed dividing $\log(\nu_p/{\rm Hz}) = 13.7$ and $\log(\nu_p/{\rm Hz}) = 14.9$ to separate LSPs, ISPs, and HSPs.

The Doppler factor is a key jet characteristic, yet we are unable to directly obtain it by observations. Fortunately, many indirect methods were proposed to estimate the Doppler factor: Lähteenmäki & Valtaoja (1999) obtained the Doppler factor from radio flux density variations. For some γ-ray-loud sources, their γ-ray emissions and timescales were also used to estimate the Doppler factor (Mattox et al. 1993; von Montigny et al. 1995; Cheng et al. 1999; Fan et al. 1999; Fan 2005; Fan et al. 2013, 2014; Pei et al. 2022). In recent years, the progress in the Doppler factor estimations has been greatly developed. Ghisellini et al. (2014) and Chen (2018) obtained the Doppler factor via the broadband SED. Liodakis et al. (2017) and Liodakis et al. (2018) compared the observed and the intrinsic brightness temperatures to derive the variability Doppler factor. Zhang et al. (2020) proposed a new method to estimate the Doppler factor for the Fermi blazars with available broad-line and γ-ray luminosities, which was updated by Zhang et al. (2023). Ye & Fan (2021) estimated the Doppler factor from the relationship between the core and extended radio luminosities. In general, different estimation methods are based on different assumptions, which result in different Doppler factor values.

Exploring the formation of relativistic jets can improve the understanding for the AGN model, but the formation is still an open question in astronomy. It is accepted that jets are produced near the central black hole, where the black hole spin (Blandford & Znajek 1977) and/or accretion disk (Blandford & Payne 1982) provide the jet power. In either case, the central black hole will continue to accrete circumnuclear material, and therefore a close correlation between the accretion luminosity and the jet power is expected (Maraschi & Tavecchio 2003). However, it is difficult to detect jet power and accretion radiation directly. To solve this problem, one can explore their relationship indirectly by other observable properties (Celotti et al. 1997; Cao & Jiang 1999; Sbarrato et al. 2012; Ghisellini et al. 2014; Xiong & Zhang 2014; Zhang et al. 2020). Because the broad-line region (BLR) clouds are photoionized by radiation from the accretion disk and then recombined, resulting in different velocity BLR lines (Kaspi et al. 2000, 2005; Bentz et al. 2009; Sbarrato et al. 2012), the BLR luminosity is used as a proxy for the accretion disk luminosity. For the jet, all of the power ($P_{\rm jet}$) commonly contains two parts, namely, the radiant power ($P_{\rm rad}$) and the kinetic power ($P_{\rm kin}$), so $P_{\rm jet} > P_{\rm rad} > \frac{L_{\rm jet}^{\rm bol}}{\Gamma^2}$, where $L_{\rm jet}^{\rm bol}$ is the jet bolometric luminosity (Sbarrato et al. 2012). The γ-ray luminosity is generally used to represent the bolometric luminosity owing to the fact that the γ-ray luminosity dominates the bolometric luminosity for the γ-ray-loud blazars (Ghisellini et al. 2014; Xiong & Zhang 2014; Zhang et al. 2020).

Ghisellini et al. (2014) found a closely linear correlation between the jet radiant power and the accretion disk luminosity, $\log P_{\rm rad} \sim 0.98 \log L_{\rm disk} + 0.639$, where $P_{\rm rad} = 2fL_{\rm jet}^{\rm bol}/\Gamma^2$, where the factor of 2 indicates two jets and f is a constant: $f = 4/3$ for BL Lacs, and $f = 16/5$ for FSRQs. The relation is consistent with the theoretical expectation. Thus, it is reasonable to represent the correlation between jet radiant power and the accretion disk luminosity by that between the γ-ray luminosity and the BLR luminosity. According to Ghisllini et al. (2014), the viewing angle of blazars is small, $\sin(\theta) \approx 1/\Gamma$, thus $\delta \approx \Gamma$. Zhang et al. (2020) proposed a new method to estimate the Doppler factor based on the correlation of the γ-ray and emission-line luminosities.

Now, a larger number of γ-ray sources are available in the fourth data release of the Fermi Large Area Telescope Fourth Source Catalog (4FGL-DR4; Ballet et al. 2023), and a large number of blazars with spectroscopic data detected by the 16th data release of the Sloan Digital Sky Survey (SDSS-DR16[7]) or the eighth data release of LAMOST (LAMOST-DR8;[8] Ahumada et al. 2020) can offer a good opportunity to reanalyze the relationship between the jet and the accretion and estimate the Doppler factor. That is the motivation for this work, which is arranged as follows: we present the sample in Section 2, our results are presented in Section 3, and discussions are given in Section 4. We then conclude our findings in the final section. Throughout this work, the cosmology constant is adopted by the ΛCDM model with $H_0 = 71$ km^{-1} s^{-1} Mpc^{-1}, $\Omega_\Lambda = 0.73$, $\Omega_M = 0.27$ (Komatsu et al. 2011).

2. The Sample

2.1. Fermi Blazars with Broad-line Emissions

Our sample consists of two parts: one part is from the literature (Paliya et al. 2021; Zhang et al. 2022), and the optical spectroscopic information of Fermi blazars is systematically compiled by Paliya et al. (2021) and Zhang et al. (2022). In the work by Paliya et al. (2021), they crossmatched the second data release of 4FGL (4FGL-DR2; Ballet et al. 2020) with the SDSS-DR16 and searched the published optical spectroscopic information of blazars in the literature, and they obtained 674 Fermi blazars with broad-line emissions. In the work by Zhang et al. (2022), there are 449 Fermi blazars with broad-line emissions from the literature: Celotti et al. (1997), Cao & Jiang (1999), Wang et al. (2004), Liu et al. (2006), Shen et al. (2011), Chai et al. (2012), Sbarrato et al. (2012), Shaw et al. (2012), Xiong & Zhang (2014), Zhang et al. (2020), and Chen et al. (2021) and references therein. Notably, 4FGL-DR4 is the latest incremental version released in 2023 late July, covering the last 14 yr of survey data. Therefore, we only considered the blazars present in the 4FGL-DR4 catalog for sources in those works (Paliya et al. 2021; Zhang et al. 2022). There are 608 and 408 sources with available BLR luminosities in the work of Paliya et al. (2021) and Zhang et al. (2022), respectively. However, there are 315 common sources in the two samples. As a consequence, we found 701 blazars in total with broad-line emissions and γ-ray emissions from the literature.

For the second part, which is derived from the matching result, they are obtained as follows: (i) We considered BL Lacs and FSRQs present in the 4FGL-DR4 catalog and prepared a preliminary sample of 1609 objects (excluding the 701 blazars with published spectroscopic information by Paliya et al. 2021 and Zhang et al. 2022). (ii) We used the associated source name in 4FGL-DR4 to search cross-identifications (cross-IDs) in the NASA/IPAC Extragalactic Database (NED)[9] one by one. (iii) We compiled their preferred position coordinates and the cross-IDs with SDSS/LAMOST prefixes. (iv) The corresponding SDSS/LAMOST name and coordinate information are used to search their optical spectra in the SDSS website or the LAMOST website. This procedure led to a sample comprising 278 spectra with broad emission lines (249 BL Lac objects and 29 FSRQs).

Finally, we obtained a total of 979 blazars (384 BL Lac objects and 595 FSRQs). Following the acronyms by Abdo et al. (2010) and the classification by Yang et al. (2022a), i.e., $\log(\nu_p/{\rm Hz}) < 13.7$ for LSPs, $13.7 < \log(\nu_p/{\rm Hz}) < 14.9$ for ISPs, and $\log(\nu_p/{\rm Hz}) > 14.9$ for HSPs, we have 518 LSPs, 212 ISPs, and 163 HSPs, or 55 LBLs, 119 IBLs, and 162 HBLs, and 463 low synchrotron peak FSRQs (LFs), 93 intermediate synchrotron peak FSRQs (IFs), and 1 (GB6 J0043+3426 with $\log\nu_p = 15.3$ Hz) high synchrotron peak FSRQ (HF) if we considered the subclasses of BL Lacs and FSRQs. The redshift of the object collected from the literature (Paliya et al. 2021; Zhang et al. 2022) was adopted, while for the 278 new Fermi

[7] https://skyserver.sdss.org/dr16/en/tools/explore/summary.aspx

[8] http://www.lamost.org/dr8/v2.0/

[9] http://ned.ipac.caltech.edu/

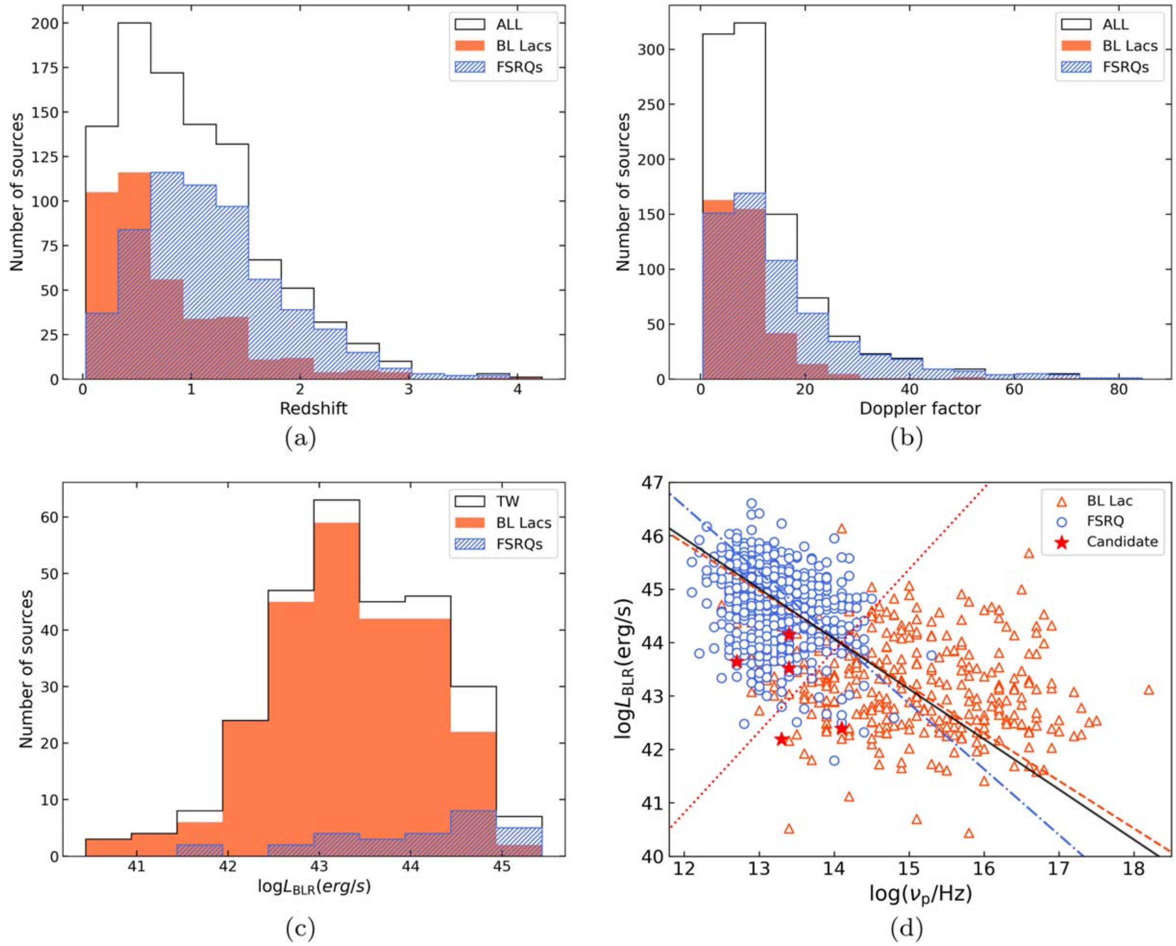

Figure 1. (a) The redshift distribution of sources, where the black histogram represents the whole sample, the orange–red histogram represents BL Lacs, and the blue histogram represents FSRQs. (b) The Doppler factor distribution. (c) The logarithm of BLR luminosity distributions for 278 blazars (black histogram). The orange–red histogram is for BL Lacs, and the blue histogram is for FSRQs. (d) The correlation between the synchrotron peak frequency ($\log(\nu_p/\mathrm{Hz})$) and the BLR luminosity ($\log L_{\mathrm{BLR}}$), where triangles stand for BL Lacs, circles for FSRQs, and stars for changing-look blazar candidates. The dotted line is a dividing line, and other straight lines correspond to the best-fitting results, the solid line to the whole sample (ALL), the dashed line to BL Lacs, and the dashed–dotted line to FSRQs.

Table 1
The Sample of 979 Fermi Blazars

4FGL Name (1)	Other Name (2)	z (3)	C_1 (4)	C_2 (5)	$\log(\nu_p/\mathrm{Hz})$ (6)	$F_{0.1-100}$ (7)	α_{ph} (8)	$\log L_\gamma$ (9)	$\log L_{\mathrm{BLR}}$ (10)	Ref. (11)	δ (12)
J0001.5+2113	TXS 2358+209	0.439	F	LSP	13.2	2.282E-11	2.67	46.31	43.65	P21	27.91
J0004.3+4614	MG4 J000421+4615	1.810	F	LSP	13.1	5.34139E-12	2.62	47.37	45.07	P21	13.79
J0004.4-4737	PKS 0002-478	0.880	F	LSP	13.0	5.24212E-12	2.40	46.41	44.10	P21	17.13
J0005.9+3824	S4 0003+38	0.229	F	LSP	13.3	6.04248E-12	2.64	45.02	42.80	TW	20.14
J0006.3-0620	PKS 0003-066	0.347	B	ISP	14.2	1.36292E-12	2.17	44.76	43.52	P21	2.06

Notes. Column (1): 4FGL name. Column (2): other name. Column (3): redshift (z). Column (4): the classification from the 4FGL-DR4 catalog (B: BL Lac; F: FSRQ). Column (5): the classification given by Yang et al. (2022a); $\log(\nu_p/\mathrm{Hz}) < 13.7$ for LSPs, $13.7 < \log(\nu_p/\mathrm{Hz}) < 14.9$ for ISPs, and $\log(\nu_p/\mathrm{Hz}) > 14.9$ for HSPs. Column (6): the synchrotron peak frequency ($\log(\nu_p/\mathrm{Hz})$) is from Yang et al. (2022a). Column (7): γ-ray flux in 0.1–100 GeV in units of erg cm^{-2} s^{-1} ($F_{0.1-100}$) is from the 4FGL-DR4 catalog. Column (8): the photon spectral index (α_{ph}) is from the 4FGL-DR4 catalog. Column (9): the logarithm of γ-ray luminosity ($\log L_{\gamma(0.1-100\ \mathrm{GeV})}$) in units of ergs per second, $\log L_\gamma$. Column (10): the logarithm of BLR luminosity in units of ergs per second, $\log L_{\mathrm{BLR}}$. Column (11): references for Column (10) (P21: Paliya et al. (2021); Z22: Zhang et al. (2022); TW: the BLR luminosity calculated in this work). Column (12): Doppler factor obtained in this work, δ.

(This table is available in its entirety in machine-readable form.)

blazars with broad emission lines we adopted the redshift information from the fourth catalog of the Fermi-LAT-detected AGNs (4LAC; Ajello et al. 2022). If the object redshift information was not found in the 4LAC, we directly used the redshift in SDSS-DR16. The redshift distribution of the sample is shown in Figure 1(a). Table 1 summarizes our blazar sample.

Column definitions in Table 1 are as follows: (1) 4FGL name; (2) other name; (3) redshift (z); (4) the classification from the 4FGL-DR4 catalog (B: BL Lac; F: FSRQ); (5) the classification given by Yang et al. (2022a; $\log(\nu_p/\mathrm{Hz}) < 13.7$ for LSPs, $13.7 < \log(\nu_p/\mathrm{Hz}) < 14.9$ for ISPs, and $\log(\nu_p/\mathrm{Hz}) > 14.9$ for HSPs); (6) the synchrotron peak frequency ($\log(\nu_p/\mathrm{Hz})$) is from Yang et al. (2022a); (7) γ-ray flux in 0.1–100 GeV in units of erg cm^{-2} s^{-1} ($F_{0.1-100}$) is from the 4FGL-DR4 catalog; (8) the photon spectral index($\alpha_{\rm ph}$) is from the 4FGL-DR4 catalog; (9) the logarithm of γ-ray luminosity (log $L_{\gamma(0.1-100\ \rm GeV)}$) in units of ergs per second, logL_γ; (10) the logarithm of BLR luminosity in units of ergs per second, log $L_{\rm BLR}$; (11) references for column (10) (P21: Paliya et al. (2021); Z22: Zhang et al. (2022); TW: the BLR luminosity calculated in this work); (12) Doppler factor obtained in this work, δ.

2.2. The Broad-line Luminosity of 278 Fermi Blazars

There are 278 γ-ray sources in our sample whose optical spectra exhibit at least one of the broad emission lines Hα, Hβ, Mg II, and C IV. To derive the broad-line luminosity, we adopted the publicly available multicomponent spectral fitting code PYQSOFit (Guo et al. 2018) and a wrapper package based on it (QSOFITMORE; Fu 2021). The tool applies the spectral models and templates to data following a χ^2-based fitting technique. A detailed description of the code and its application can be found in Guo et al. (2018), Shen et al. (2019), and Fu (2021).

Based on the extinction curves from Cardelli et al. (1989) and the dust map of Schlegel et al. (1998), we first corrected the Galactic reddening for the target spectrum, and then a fitting was performed. The spectrum was decomposed into two components, namely the quasar and the host galaxy components, following the principal component analysis method presented in Yip et al. (2004a, 2004b). In order to efficiently fit the line-free continuum over the entire spectrum, four components are considered, namely a power law and a third-order polynomial along with optical and Fe II templates (Boroson & Green 1992; Vestergaard & Wilkes 2001; Shen et al. 2019). Afterward, we can obtain a line-only spectrum using the spectrum to subtract the best-fitted continuum, where the spectral properties of Hα, Hβ, Mg II, and C IV emission lines were extracted.

We fitted Hα and Hβ emission lines in the wavelength range [6400, 6800] Å and [4640, 5100] Å, respectively. The broad components of Hα and Hβ were modeled by three Gaussian profiles; the narrow components of Hα and Hβ, [N II] $\lambda\lambda$6549, 6585, and [S II] $\lambda\lambda$6718, 6732 were each modeled by a single Gaussian profile (Shen et al. 2019).

The Mg II and C IV line fittings were carried out in the wavelength range [2700, 2900] Å and [1500, 1700] Å, respectively. We used two Gaussians and a single Gaussian to model the broad and narrow components of the Mg II line, respectively. The broad component of the C IV line was modeled with three Gaussians (Shen et al. 2019).

In this way, we obtained the flux of at least one of Hα, Hβ, Mg II, and C IV emission lines and calculated the corresponding luminosity of the broad emission line (Zhang et al. 2020):

$$L_\lambda = 4\pi d_L^2 \lambda F(\lambda), \tag{1}$$

where $d_L = (1+z)\cdot \frac{c}{H_0}\cdot \int_1^{1+z} \frac{1}{\sqrt{\Omega_M x^3 + 1 - \Omega_M}}dx$ is luminosity distance and $\lambda F(\lambda)$ is the flux density in units of erg cm^{-2} s^{-1}. We show, as examples, the fitting results in Figure 2.

In addition, we calculated the BLR luminosity from the available observational data as follows (Zhang et al. 2020; Paliya et al. 2021; Zhang et al. 2022):

$$L_{\rm BLR} = L_{i,\rm obs}\frac{\langle L_{\rm BLR}\rangle}{L_{i,\rm est}}, \tag{2}$$

where $\langle L_{\rm BLR}\rangle$ is the total BLR fraction. We typically take $\langle L_{\rm BLR}\rangle = 5.56 L_{y\alpha}$ and set $L_{y\alpha} = 100$, and then we sum the line ratios (relative to $L_{y\alpha}$) as in Francis et al. (1991) and Celotti et al. (1997). $L_{i,\rm obs}$ are the observed luminosities obtained from a certain number of broad lines, and $L_{i,\rm est}$ are the luminosities obtained from the same lines but estimated from the line ratios that are adopted: 77, 22, 34, and 63 for Hα, Hβ, Mg II, and C IV, respectively (Francis et al. 1991; Celotti et al. 1997). When there are two or more emission lines for a source, we will use their geometric mean as the BLR luminosity. For the 278 Fermi blazars, the logarithm of the BLR luminosity (log$L_{\rm BLR}$) is listed in Table 2 and shown in Figure 1(c).

3. Results

3.1. The Averaged BLR Luminosity

For the sample, we calculated their average logarithm of observed BLR luminosity for BL Lacs, FSRQs, LSPs, ISPs, HSPs, LBLs, IBLs, and HBLs and obtained the following statistical results. The corresponding average values are listed in Table 3. When we considered BL Lacs and FSRQs separately, we found that the BLR luminosity ranges from log$L_{\rm BLR}$ = 40.44 to 46.14 erg s^{-1} with an average value of log$L_{\rm BLR}$ = 43.28 erg s^{-1} for the 384 BL Lacs and from log$L_{\rm BLR}$ = 41.79 to 46.61 erg s^{-1} with an average value of log$L_{\rm BLR}$ = 44.70 erg s^{-1} for the 595 FSRQs. It is observed that the BLR luminosity in FSRQs is higher than that in BL Lacs.

If we considered LSPs, ISPs, and HSPs separately, we can find that their average logarithms of the BLR luminosity are 44.67, 43.80, and 43.09 erg s^{-1}, respectively. For LBLs, IBLs, and HBLs, the average observed BLR luminosities are 43.65, 43.37, and 43.08 erg s^{-1}, respectively. The statistic results and distributions are shown in Table 3 and Figure 3.

3.2. The Correlation between the Synchrotron Peak Frequency and BLR Luminosity

When the ordinary and symmetrical least-squares regression (OLS[10]; Feigelson & Babu 1992) is employed for the BLR luminosity and the synchrotron peak frequency, an anticorrelation:

$$\log L_{\rm BLR} = -(0.94 \pm 0.02)\log \nu_p + (57.23 \pm 0.34)$$

with a correlation coefficient of $r = -0.60$ and a chance probability of $p < 10^{-4}$ was obtained for the whole sample and listed in Table 4, in which other results are also listed.

3.3. The Correlation between the γ-Ray Luminosity and the BLR Luminosity

To investigate the correlation between the γ-ray and the BLR Luminosities, we first calculated the γ-ray luminosity by (Lin et al. 2017; Xiao et al. 2022d)

$$L_\gamma = 4\pi d_L^2 (1+z)^{\alpha_{\rm ph}-2} F, \tag{3}$$

[10] https://astrostatistics.psu.edu/statcodes/sc_regression.html

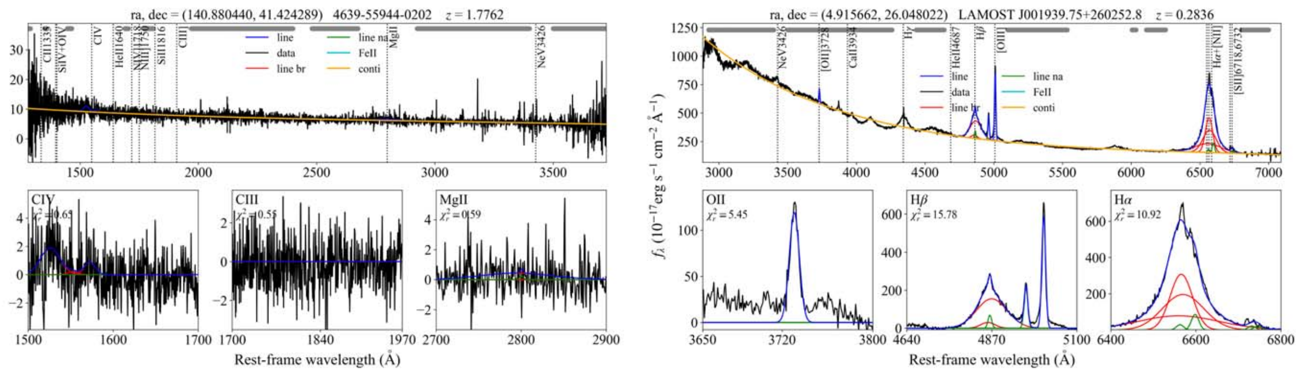

(a) (b)

Figure 2. The optical spectra of B3 0920+416 or 4FGL J0923.5+4125 (left) and 4C +25.01 or 4FGL J0018.8+2611 (right) modeled with QSOFITMORE. The spectral data are shown with the black line. Red and green lines represent broad and narrow components of the emission line, respectively, and the modeled continuum is plotted with the orange line. The blue line is the sum of all the components. Horizontal gray dashes at the top of the plots denote the line-free wavelength regions selected to model the continuum emission. The data are adopted from SDSS-DR16 for B3 0920+416 and LAMOST-DR8 for 4C +25.01.

Table 2
The Sample of 278 Fermi Blazars

4FGL Name (1)	z (2)	Class (3)	$f_{\mathrm{H}\alpha}$ (4)	$f_{\mathrm{H}\beta}$ (5)	$f_{\mathrm{Mg\ II}}$ (6)	$f_{\mathrm{C\ IV}}$ (7)	$\log L_{\mathrm{BLR}}$ (8)
J0005.9+3824	0.229	F	1093.92 ± 170.54	86.04 ± 9.15			42.80 ± 0.04
J0009.1+0628	1.563	B		29.06 ± 15.61	196.79 ± 18.26		44.39 ± 0.12
J0013.0+3355	1.682	F			41.81 ± 18.48	712.36 ± 44.39	44.60 ± 0.10
J0014.2+0854	0.163	B		119.29 ± 21.22			42.33 ± 0.08
J0018.8+2611	0.280	F	62566.31 ± 542.46	19027.08 ± 1454.89			45.05 ± 0.02

Note. Column (1): 4FGL name. Column (2): redshift (z). Column (3): classification (B: BL Lac; F: FSRQ). Column (4): Hα emission line flux in units of 10^{-17} erg^{-1} cm^{-2}; Column (5): Hβ emission line flux in units of 10^{-17} erg^{-1} cm^{-2}. Column (6): Mg II emission-line flux in units of 10^{-17} erg^{-1} cm^{-2}. Column (7): C IV emission-line flux in units of 10^{-17} erg^{-1} cm^{-2}. Column (8): logarithm of the BLR luminosity in units of ergs per second (log L_{BLR}).

(This table is available in its entirety in machine-readable form.)

Table 3
Statistical Results for the Broad-line Luminosities

Source (1)	BL Lac (2)	FSRQ (3)	HSP (4)	ISP (5)	LSP (6)	HBL (7)	IBL (8)	LBL (9)
Number	384	595	163	212	518	162	119	55
Minimum	40.44	41.79	40.44	41.12	40.52	40.44	42.12	40.52
Maximum	46.14	46.61	45.68	46.14	46.61	45.68	46.14	45.22
Median	43.28	44.81	42.97	43.94	44.8	42.97	43.32	43.71
Mean	43.22	44.7	43.09	43.8	44.67	43.08	43.37	43.65

Note. Column (1): statistical parameters. Column (2): parameter for the BL Lacertae object (BL Lacs). Column (3): parameter for the flat-spectrum radio quasar (FSRQ). Column (4): parameter for the high synchrotron peak (HSP) blazars. Column (5): parameter for the intermediate synchrotron peak (ISP) blazars. Column (6): parameter for the low synchrotron peak (LSP) blazars. Column (7): parameter for the high synchrotron peak BL Lacs (HBL). Column (8): parameter for the intermediate synchrotron peak BL Lacs (IBL). Column (9): parameter for the low synchrotron peak BL Lacs (LBL).

where z is redshift, $(1+z)^{\alpha_{\mathrm{ph}}-2}$ is a K-correction, α_{ph} is the photon spectral index, and F is the integral flux in erg cm^{-2} s^{-1}. In this work, the energy flux in 0.1–100 GeV is adopted from 4FGL-DR4.[11] The logarithm of the γ-ray luminosity is listed in Table 1. When the OLS bisector regression was performed for the γ-ray luminosity and the BLR luminosity of sources, we obtained the results

$$\log L_{\gamma} = (1.03 \pm 0.02)\log L_{\mathrm{BLR}} + (0.94 \pm 0.77)$$

with $r = 0.81$ and $p < 10^{-4}$ for the 979 blazars. The corresponding result is shown in Figure 4 and listed in Table 4.

[11] https://fermi.gsfc.nasa.gov/ssc/data/access/lat/14yr_catalog/

3.4. Estimation of the Doppler Factor

Since the viewing angle of blazars is small, sin (θ) $\approx 1/\Gamma$, so $\delta \approx \Gamma$. The jet radiation power can be expressed as (Ghisellini et al. 2014)

$$P_{\mathrm{rad}} = 2fL_{\mathrm{jet}}^{\mathrm{bol}}/\delta^{2}, \tag{4}$$

and Ghisellini et al. (2014) found that the nonthermal radiation is closely related to the disk luminosity as $\log P_{\mathrm{rad}} \sim 0.98\log L_{\mathrm{disk}} + 0.639$ for a sample of 217 blazars. Zhang et al. (2020) considered BL Lacs and FSRQs in Ghisellini et al. (2014) separately with the OLS bisector regression and obtained the correlation between the P_{rad} and L_{disk} and the

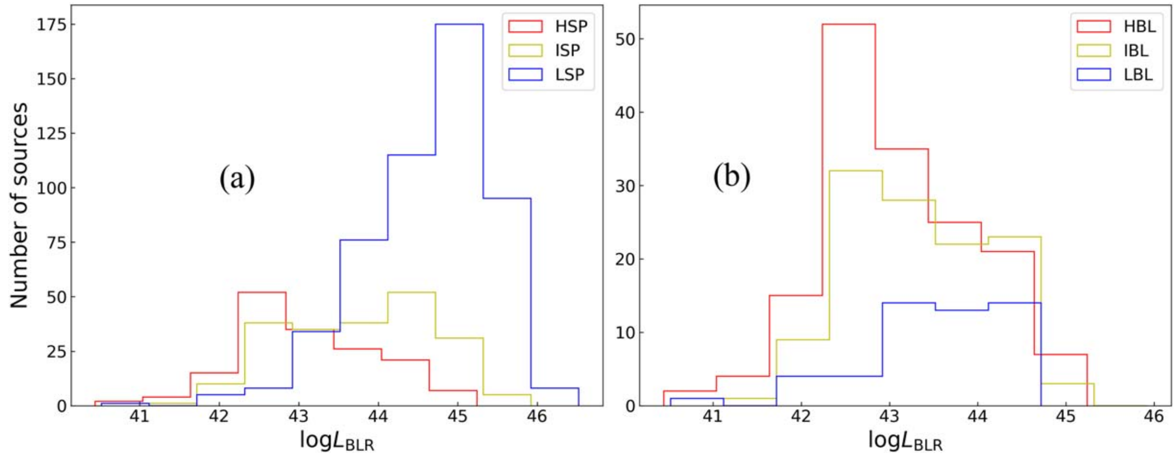

Figure 3. (a) The broad-line luminosities for blazars with different synchrotron peak; the red line is for the high synchrotron peak (HSP) blazars, the yellow line is for the intermediate synchrotron peak (ISP) blazars, and the blue line is for the low synchrotron peak (LSP) blazars. (b) The broad-line luminosities for BL Lacs with different synchrotron peak; the red line is for the high synchrotron peak BL Lacs (HBLs), the yellow line is for the intermediate synchrotron peak BL Lacs (IBLs), and the blue line is for the low synchrotron peak BL Lacs (LBLs).

Table 4
Linear Regression Fitting Results

Y (1)	X (2)	Source (3)	N (4)	$a \pm \Delta a$ (5)	$b \pm \Delta b$ (6)	r (7)	p (8)
$\log L_\gamma$	$\log L_{\rm BLR}$	TW	278	0.999 ± 0.031	2.329 ± 1.361	0.82	<0.0001
$\log L_\gamma$	$\log L_{\rm BLR}$	G14	182	1.080 ± 0.046	-1.401 ± 2.171	0.71	<0.0001
$\log L_\gamma$	$\log L_{\rm BLR}$	X14	215	1.062 ± 0.044	-0.321 ± 1.987	0.68	<0.0001
$\log L_\gamma$	$\log L_{\rm BLR}$	P21	672	1.150 ± 0.029	-4.605 ± 1.302	0.67	<0.0001
$\log L_\gamma$	$\log L_{\rm BLR}$	Z22	442	1.110 ± 0.028	-3.011 ± 1.289	0.72	<0.0001
$\log L_\gamma$	$\log L_{\rm BLR}$	ALL	979	1.027 ± 0.017	0.941 ± 0.769	0.81	<0.0001
$\log L_\gamma$	$\log \delta$	G14	182	8.813 ± 1.408	37.282 ± 1.535	0.37	<0.0001
$\log L_\gamma$	$\log \delta$	C18	580	1.334 ± 0.153	45.088 ± 0.165	0.10	0.014
$\log L_\gamma$	$\log \delta$	L18	353	1.892 ± 0.127	44.705 ± 0.164	0.40	<0.0001
$\log L_\gamma$	$\log \delta$	ALL	979	2.752 ± 0.081	43.644 ± 0.078	0.56	<0.0001
$\log L_{\rm BLR}$	$\log \nu_{\rm p}$	Blazars	893	-0.941 ± 0.021	57.231 ± 0.342	-0.60	<0.0001
$\log L_{\rm BLR}$	$\log \nu_{\rm p}$	BL Lacs	336	-0.892 ± 0.031	56.541 ± 0.441	-0.27	<0.0001
$\log L_{\rm BLR}$	$\log \nu_{\rm p}$	FSRQs	557	-1.233 ± 0.053	61.312 ± 0.612	-0.29	<0.0001

Note. Column (1): dependent variable (the γ-ray luminosity). Column (2): independent variable (the BLR luminosity or the Doppler factor). Column (3): references for independent variables: TW: the BLR luminosity calculated in this work for the 278 sources; G14: Ghisellini et al. (2014); X14: Xiong & Zhang (2014); C18: Chen (2018); L18: Liodakis et al. (2018); P21: Paliya et al. (2021); Z22: Zhang et al. (2022); ALL: 979 sources with BLR luminosity in this work. Column (4): the number of sources. Column (5): slope. Column (6): intercept. Column (7): the correlation coefficient. Column (8): the chance probability.

Doppler factor estimation formula by setting $L_{\rm disk} = 10 L_{\rm BLR}$ and $L_{\rm jet}^{\rm bol} = L_{\rm jet}$:

$$\log \delta = 0.5(\log L_\gamma - 1.178 \log L_{\rm BLR} + 8.004) \quad (5)$$

for FSRQs and

$$\log \delta = 0.5(\log L_\gamma - 0.870 \log L_{\rm BLR} - 6.266) \quad (6)$$

for BL Lacs.

Therefore, for a blazar with available γ-ray and BLR luminosities, one can estimate its Doppler factor. In this work, based on the available luminosities, we obtained the Doppler factors for the 979 Fermi blazars and listed them in Table 1. Parameter δ is found to range from 0.45 for 4FGL J0332.1−1123 to 88.52 for TXS 0106+612 with an average value of $\langle \delta \rangle = 12.99$ for the whole sample. If we considered FSRQs and BL Lacs separately, their range and average values are $\delta = 0.45$ for 4FGL J0332.1−1123 to 88.52 for TXS 0106+612 with $\langle \delta \rangle = 15.75$ for FSRQs and $\delta = 1.13$ for 4FGL J0843.1+5034 to 66.89 for PKS 0426−380 with $\langle \delta \rangle = 8.14$ for BL Lacs, and the distributions of the Doppler factors are shown in Figure 1(b). In addition, we collected the Doppler factors from Ghisellini et al. (2014), Chen (2018), and Liodakis et al. (2018) for comparisons.

4. Discussions

4.1. The Correlations

The relationship between the jet power and the accretion luminosity was discussed in the literature (Maraschi & Tavecchio 2003; Punsly & Tingay 2006; Celotti & Ghisellini 2008; Ghisellini et al. 2010, 2014; Zhang et al. 2020, 2022). In the present work, we used a larger sample to revisit the relation using γ-ray luminosity and the BLR luminosity. By the OLS method, we obtained a strong correlation $\log L_\gamma = (1.03 \pm 0.02) \log L_{\rm BLR} + (0.94 \pm 0.77)$ with $r = 0.81$ and $p < 10^{-4}$ for the 979 sources as shown in Figure 4 and Table 4.

For comparison, we also studied the correlation between γ-ray luminosity calculated in this work from the 4FGL-DR4 and BLR luminosity for sources in the literature (Ghisellini et al. 2014; Xiong & Zhang 2014; Paliya et al. 2021; Zhang et al. 2022); we

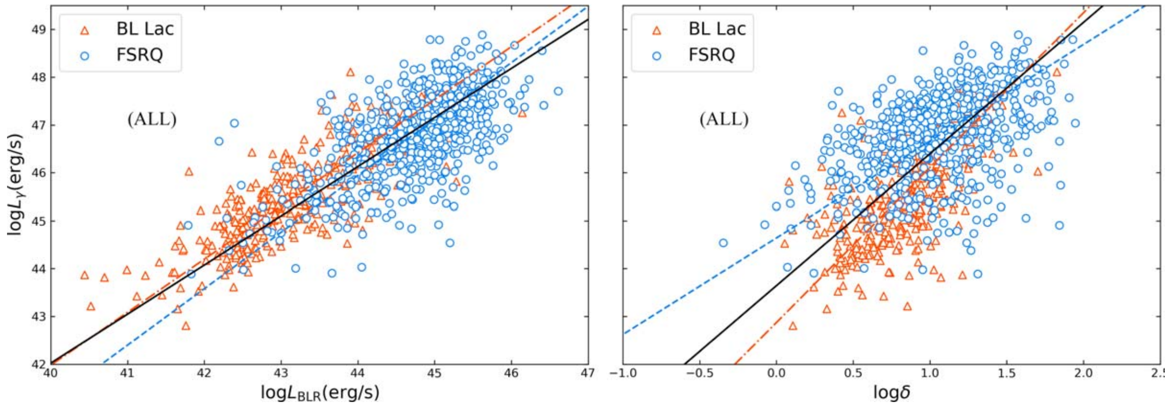

Figure 4. The left panel shows the γ-ray luminosity vs. the broad-line luminosity, and the right panel shows the γ-ray luminosity vs. the Doppler factor, where triangles stand for BL Lacs and circles for FSRQs. The straight lines correspond to the best-fitting results: the solid line to the whole sample (ALL), the dashed line to BL Lacs, and the dashed–dotted line to FSRQs.

only considered the sources present in the 4FGL-DR4 catalog and then obtained $\log L_\gamma = (1.119 \pm 0.058)\log L_{\rm BLR} - (2.885 \pm 2.578)$ with $r = 0.71$ and $p < 10^{-4}$ for 182 sources from Ghisellini et al. (2014), $\log L_\gamma = (1.062 \pm 0.044) \log L_{\rm BLR} - (0.321 \pm 1.987)$ with $r = 0.68$ and $p < 10^{-4}$ for 215 sources from Xiong & Zhang (2014), $\log L_\gamma = (1.150 \pm 0.029)\log L_{\rm BLR} - (4.605 \pm 1.302)$ with $r = 0.67$ and $p < 10^{-4}$ for 672 sources from Paliya et al. (2021), and $\log L_\gamma = (1.110 \pm 0.028)\log L_{\rm BLR} - (3.011 \pm 1.289)$ with $r = 0.72$ and $p < 10^{-4}$ for 442 sources from Zhang et al. (2022). This shows that the correlation results obtained from the 979 sources are consistent with previous works (Ghisellini et al. 2014; Xiong & Zhang 2014; Paliya et al. 2021; Zhang et al. 2022). The fitting results are listed in Table 4.

From Equations (1) and (3), it is obvious that the redshift is a key parameter in luminosity calculations. In this work, there are 979 Fermi blazars, 88 of whose redshifts are from SDSS-DR16 spectra. However, some sources have bad χ^2 in the redshift estimations from the SDSS spectra. We studied the relationship between the broad-line luminosity ($\log L_{\rm BLR}$) and γ-ray luminosity ($\log L_\gamma$) for the 88 sources with redshifts from SDSS and 891 (979 − 88) sources, respectively, to explore the effect of the 88 sources on the results, and obtained

$$\log L_\gamma = (1.02 \pm 0.05)\log L_{\rm BLR} + (1.38 \pm 2.3)$$

with $r = 0.84$ and $p < 10^{-4}$ for the 88 sources with redshifts from SDSS-DR16 spectra and

$$\log L_\gamma = (1.03 \pm 0.02)\log L_{\rm BLR} + (0.69 \pm 0.80)$$

with $r = 0.80$ and $p < 10^{-4}$ for a sample of 891 sources (excluding the 88 sources with redshifts from SDSS spectra). As shown in Figure 5, we found that the relationship between broad-line luminosity and γ-ray luminosity is very consistent in slopes and not much different in intercepts when the uncertainties are taken into account in both cases. This indicates that the redshift does not have much effect on our results.

The beaming effect of Fermi blazars has also been discussed (Kovalev et al. 2009; Arshakian et al. 2010; Fan et al. 2017; Yang et al. 2022b). We found a positive correlation between the γ-ray luminosity and the Doppler factor, $\log L_\gamma = (2.752 \pm 0.081)\log \delta + (43.644 \pm 0.078)$ with $r = 0.56$ and $p < 10^{-4}$, by the OLS method, which is shown in Figure 4 and Table 4, in which we also listed the correlation analysis results obtained from the γ-ray luminosity and the Doppler factors

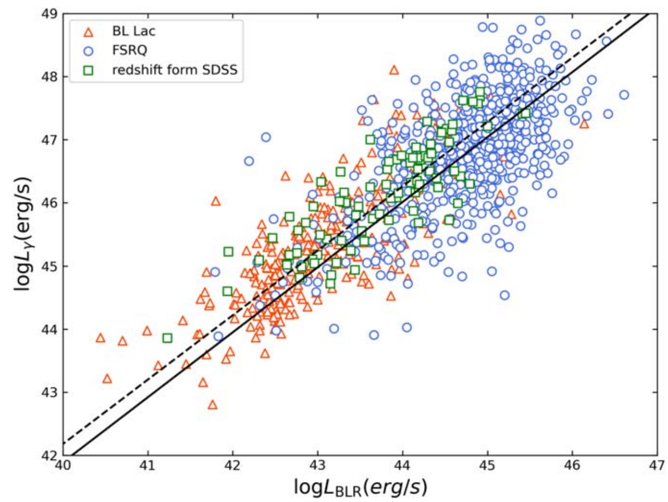

Figure 5. The γ-ray luminosity vs. the broad-line luminosity, where triangles stand for BL Lacs, circles for FSRQs, and squares for 88 blazars with redshifts from SDSS spectra. The straight lines correspond to the best-fitting results: the dashed line to the 88 blazars, the solid line to the 891 sources excluding the 88 blazars with redshifts from SDSS spectra (979 − 88).

from the literature (Ghisellini et al. 2014; Chen 2018; Liodakis et al. 2018). All the fitting results in Table 4 suggest that the γ-ray luminosity and the Doppler factor are positively correlated, though different estimation methods are used to obtain the Doppler factors, suggesting that the γ-rays are beamed.

4.2. A New Dividing Line between BL Lacs and FSRQs

Blazars, a unique subclass of AGNs, exhibit distinct SEDs featuring two peaks. The first peak, known as the synchrotron peak, spans the electromagnetic spectrum from the infrared to the X-ray range. It predominantly arises from the synchrotron emission. The second peak, referred to as the inverse Compton peak, extends from the X-ray to the γ-ray wavelengths. This peak is believed to originate from the process of inverse Compton scattering. Fossati et al. (1998) found that 5 GHz radio luminosity, synchrotron peak luminosity, and γ-ray luminosity all exhibited inverse relationships with the synchrotron peak frequency and that the synchrotron peak frequency increased while the luminosity consistently decreased. This finding has led to a blazar sequence, ranging from FSRQs to X-ray-selected BL Lacs, with luminosity decreasing as the peak frequency increases. Mao et al. (2016) obtained SEDs for a substantial selection of Roma-BZCAT blazars. Interestingly, their findings echoed those of Fossati et al. (1998), revealing a blazar sequence. They found that as radio (and bolometric/integrated synchrotron) luminosity decreased, the peak frequency consistently increased. Later on, Fan et al. (2017) calculated the intrinsic SEDs for a sample of 86 Fermi blazars. They identified an inverse relationship between the luminosity (across radio, optical, X-rays, γ-rays, and the synchrotron peak) and the peak frequency when examining the observed data. When considering the intrinsic data, the correlation exhibited a positive trend. Yang et al. (2022b) revisited the correlations between the γ-ray (or radio, optical, X-ray, peak frequency, integrated synchrotron) luminosity and the synchrotron peak frequency with a larger sample of 260 Fermi blazars and confirmed the results by Fan et al. (2017). It is clear that the relationship between the multiband luminosities and the synchronized peak frequencies had been extensively investigated. However, there is not much discussion about the correlation between the BLR luminosity and the synchrotron peak frequency.

Here we plotted BL Lacs and FSRQs on a plot of the BLR luminosity versus the synchrotron peak frequency and found a significant anticorrelation between them and that FSRQs and BL Lacs clearly occupy different regions (see Table 4 and Figure 1(d)). In order to effectively separate these two classes, we employed a kind of machine-learning (ML) method to establish a dividing line. Recently, ML methods, such as support vector machine (SVM), artificial neural networks, K-nearest neighbors, etc., have been widely used in astronomy; see Kang et al. (2019), Kovačević et al. (2019), Xu et al. (2020), Zhu et al. (2021), Xiao et al. (2022b, 2022c, 2023), and Zhu et al. (2023). The SVM model can easily handle both linear and nonlinear classification problems by choosing different kernel functions. The model is relatively simple, especially in linearly separable cases, making the decision boundary intuitively interpretable. In this work, based on the sample distribution, we chose a linear kernel function and used a cross-validation to determine the optimal penalty parameter ($C = 1$). Then, we got a dividing line with an accuracy rate of 90.73%, which is expressed as

$$\log L_{\rm BLR} = 1.58 \log \nu_p - 19.46.$$

We found that the BL Lacs located above the dividing line exhibit higher BLR emissions than the BL Lacs below the line. According to blazar evolution (Böttcher & Dermer 2002), we proposed that those BL Lacs are in the early stages of transitioning from FSRQs to BL Lacs. At this phase, the central black hole is surrounded by abundant gas and dust, enabling the black hole to show a high accretion rate and enhancing radiation from the core region. Thus, the BLR clouds are effectively photoionized by radiation from the accretion disk and then recombined, resulting in different velocity BLR lines. Meanwhile, the high energy density in the external radiation field will enhance the level of Compton cooling, which leads to lower synchrotron peak frequencies (Ghisellini et al. 1998). The objects in this case are located in the upper left corner of Figure 1(d). In contrast, the average density of the circumnuclear material will gradually decrease with further evolution. This will lead to a decreasing accretion rate and a decreasing level of Compton cooling. The objects gradually move toward the lower right corner of Figure 1(d).

4.3. The Doppler Factor

In this work, we compiled 979 Fermi blazars with γ-ray and BLR luminosities and computed the Doppler factor by taking the γ-ray luminosity as the jet bolometric luminosity (Zhang et al. 2020). We can get the Doppler factor to be in the range of 0.45–358.06. Notably, there are six FSRQs, namely S5 1044+71, B3 0920+416, PMN J0641–0320, B2 0218+35, PKS 1758–651, and TXS 0106+612, and their Doppler factors are 93.57, 94.74, 126.55, 130.41, 301.77, and 358.06, respectively; their BLR luminosities are 44.15, 43.59, 43.52, 43.64, 42.19, and 42.39 erg s^{-1}, respectively. We believed those Doppler factors to be overestimated, due to two possible reasons.

On the one hand, the spectral information is not accurate. In Paliya et al. (2021), a part of the spectrum data is obtained by digitizing a plot from the historical literature. This will reduce the resolution of the emission lines, making the emission-line intensity become smaller. We found only one corresponding SDSS spectrum (B3 0920+416) for the six objects; it is shown in Figure 2(a).

On the other hand, the sources may be transition objects between BL Lacs and FSRQs. Xiao et al. (2022a) reported their EWs as follows: $\mathrm{EW_{Mg\ II}} = 8.31 \pm 9.69$ and $\mathrm{EW_{C\ IV}} = 10.43 \pm 2.51$ for B3 0920+416, $\mathrm{EW_{Mg\ II}} = 9.03 \pm 3.78$ for TXS 0106+612, $\mathrm{EW_{Mg\ II}} = 13.61 \pm 11.97$ for S5 1044+71, $\mathrm{EW_{Mg\ II}} = 40.89 \pm 7.5$ for B2 0218+35, $\mathrm{EW_{Mg\ II}} = 93.59 \pm 20.41$ for PMN J0641−0320, and $\mathrm{EW_{Mg\ II}} = 153.54 \pm 7.3$ for PKS 1758−651. In addition, we also fitted one SDSS spectrum (B3 0920+416; see Figure 2(a)), and we got $\mathrm{EW_{Mg\ II}} = 7.4 \pm 2.2$ and $\mathrm{EW_{C\ IV}} = 7.8 \pm 2.1$ for B3 0920+416. The EWs of the first three FSRQs (TXS 0106+612, S5 1044+71, and B2 0218+35) were very small, and B3 0920+416 was confirmed to be a transition object (Shaw et al. 2012).

We thought that the six sources are similar to the changing-look AGNs (CL AGNs), which have recently attracted the attention of many astronomers. CL AGNs can exhibit a transition from Type 1 to Type 1.8, 1.9, and 2 or vice versa, featuring disappearing or emerging broad emission lines on timescales of months to years (LaMassa et al. 2015; MacLeod et al. 2016; Gezari et al. 2017; Sheng et al. 2020; Peña-Herazo et al. 2021; Xiao et al. 2022a). In particular, Cohen et al. (1986) found that Mrk 1018 transitioned from Seyfert 1.9 to Seyfert 1 and then back to Seyfert 1.9 (McElroy et al. 2016). The changing-look mechanism also exists in blazars (Foschini et al. 2021; Peña-Herazo et al. 2021). Therefore, we suggested that the five FSRQs (S5 1044+71, PMN J0641−0320, B2 0218+35, PKS 1758−651, and TXS 0106+612) can be candidates for CL AGNs. Considering them (including B3 0920+416) as BL Lacs in our work is reasonable. If we take B3 0920+416, PMN J0641−0320, B2 0218+35, PKS 1758−651, and TXS 0106+612 as BL Lacs, then from Equation (6) we can get Doppler factors of 43.18, 35.84, 46.70, 50.22, 69.49, and 88.52, respectively. In this case, the Doppler factor ranges from $\delta = 0.45$ to 88.52 with a mean value of 12.99 for the 979 Fermi blazars.

As mentioned earlier, the Doppler factor is a key parameter for the jet, but it is very hard to observe directly. Many different methods were proposed for Doppler factor estimation; see, e.g., Ghisellini et al. (1993), Cheng et al. (1999), Fan et al. (1999), Fan (2005), Fan et al. (2009, 2013, 2014), Ghisellini et al. (2014), Chen (2018), Liodakis et al. (2018), Zhang et al. (2020), Ye & Fan (2021), and Zhang et al. (2023). Ghisellini et al. (2014) took an estimation from SED modeling for the Doppler factor and considered $\delta \approx \Gamma$ for blazars; it is found that the narrow distribution of the Doppler factor peaks at $\delta = \Gamma \sim 13 \pm 1.4$ for 217 blazars. Chen (2018) obtained the Doppler factors for 999 sources; δ is in the range of 1–99.5 with $\langle\delta\rangle = 17.61$. Liodakis et al. (2018) obtained the variability Doppler factors for 878 sources (670 FSRQs, 118 BL Lacs, 33 radio galaxies, and 57 uncertain sources), the average value is $\langle\delta\rangle = 14$. Zhang et al. (2020) proposed a new approach to obtain the Doppler factor based on the correlation between the radiation power of the jet and the BLR luminosities; their results showed that δ was in the range of 0.35–85.66 with $\langle\delta\rangle = 12.54$. We also compared the Doppler factors from those works with ours. The compared results are shown below.

There are 182 common sources with Ghisellini et al. (2014). For the 182 sources from Ghisellini et al. (2014), δ is in the range of 5–18 with a mean value of $\langle\delta\rangle = 12.00$; their mean values are $\langle\delta\rangle = 11.00$ and $\langle\delta\rangle = 13.00$ for BL Lacs and FSRQs, respectively. For the 182 sources in this work, δ is in the range of 2.24–71.25 with a mean value of $\langle\delta\rangle = 17.12$; their mean values are $\langle\delta\rangle = 13.68$ and $\langle\delta\rangle = 17.80$ for BL Lacs and FSRQs, respectively.

There are 582 common sources with Chen (2018). For the 582 sources from Chen (2018), δ is in the range of 1.00–99.50 with $\langle\delta\rangle = 16.65$; their mean values are $\langle\delta\rangle = 21.87$ and $\langle\delta\rangle = 13.57$ for BL Lacs and FSRQs, respectively. For the 582 sources in this work, δ is in the range of 1.21–88.52 with a mean value of $\langle\delta\rangle = 14.56$; their mean values are $\langle\delta\rangle = 10.41$ and $\langle\delta\rangle = 40.96$ for BL Lacs and FSRQs, respectively.

There are 353 common sources with Liodakis et al. (2018). For the 353 sources from Liodakis et al. (2018), δ is in the range of 0.23–88.44 with $\langle\delta\rangle = 16.86$; their mean values are $\langle\delta\rangle = 13.97$ and $\langle\delta\rangle = 17.37$ for BL Lacs and FSRQs, respectively. For the 353 sources in this work, δ is in the range of 0.84–88.84 with a mean value of $\langle\delta\rangle = 16.18$; their mean values are $\langle\delta\rangle = 13.13$ and $\langle\delta\rangle = 16.72$ for BL Lacs and FSRQs, respectively. In Ghisellini et al. (2014), Liodakis et al. (2018), and this work, the average Doppler factor of the FSRQs is higher than that of the BL Lacs; however, this is reversed in Chen (2018). We think that it is not true to assume $\Delta t/(1+z) \approx 1$ day for all sources in Chen (2018).

5. Conclusions

In this paper, we obtained a total of 979 Fermi blazars (595 FSRQs and 384 BL Lacs) with emission lines. We studied the correlations between the BLR luminosities and both the γ-ray luminosities and the synchrotron peak frequency, and then we estimated the Doppler factor for all those Fermi blazars. We made a linear correlation analysis between the γ-ray luminosity and the Doppler factor, and we made the Doppler factor comparisons with the available results from the literature. In addition, we proposed a new dividing line separating BL Lacs and FSRQs. Our conclusions are as follows:

(1) We calculated the broad-line luminosities for 278 objects from SDSS or LAMOST. Their logarithms of broad-line luminosities are in the range of 40.44–45.45 erg s^{-1} with a mean value of 43.39 erg s^{-1} for the 278 objects.

(2) Doppler factors are found to be in the range of $\delta = 0.45$–88.52 for the 979 Fermi blazars. The average values of the Doppler factors are $\delta = 15.75$ and $\delta = 8.71$ for FSRQs and BL Lacs, respectively. The Doppler factor in BL Lacs is, on average, smaller than that in FSRQs, which is consistent with those obtained in Ghisellini et al. (2014) and Liodakis et al. (2018).

(3) The γ-ray luminosity is positively correlated with both the broad-line luminosity and the Doppler factor. The broad-line luminosity is anticorrelated with synchrotron peak frequency, which could be due to Compton cooling.

(4) We proposed that the five FSRQs (S5 1044+71, PMN J0641–0320, B2 0218+35, PKS 1758–651, and TXS 0106 +612) are candidates for changing-look blazars.

Acknowledgments

We thank the anonymous reviewer for the constructive suggestions and comments. The work is partially supported by the National Natural Science Foundation of China (NSFC U2031201, NSFC 11733001, NSFC 12303018) and the Guangdong Major Project of Basic and Applied Basic Research (grant No. 2019B030302001). We also acknowledge the Scientific and Technological Cooperation Projects (2020–2023) between the People's Republic of China and the Republic of Bulgaria, the science research grants from the China Manned Space Project with No. CMS-CSST-2021-A06, and the supports for Astrophysics Key Subjects of Guangdong Province and Guangzhou City. The work is also supported by the Key Laboratory for Astronomical Observation and Technology of Guangzhou.

ORCID iDs

Guohai Chen https://orcid.org/0009-0006-2844-8677
Xiangtao Zeng https://orcid.org/0000-0002-0551-5615
Lixia Zhang https://orcid.org/0000-0003-3184-6896
Hubing Xiao https://orcid.org/0000-0001-8244-1229
Xiang Liu https://orcid.org/0000-0001-9815-2579
Lang Cui https://orcid.org/0000-0003-0721-5509
Junhui Fan https://orcid.org/0000-0002-5929-0968

References

Abdo, A. A., Ackermann, M., Ajello, M., et al. 2010, ApJ, 723, 1082
Ahumada, R., Allende Prieto, C., Almeida, A., et al. 2020, ApJS, 249, 3
Ajello, M., Baldini, L., Ballet, J., et al. 2022, ApJS, 263, 24
Aller, H. D., Aller, M. F., Plotkin, R. M., Hughes, P. A., & Hodge, P. E. 2003, AAS Meeting, 203, 63.05
Andruchow, I., Romero, G. E., & Cellone, S. A. 2005, A&A, 442, 97
Arshakian, T. G., León-Tavares, J., Torrealba, J., & Chavushyan, V. H. 2010, arXiv:1006.2079
Ballet, J., Bruel, P., Burnett, T. H., Lott, B. & The Fermi-LAT Collaboration 2023, arXiv:2307.12546
Ballet, J., Burnett, T. H., Digel, S. W., & Lott, B. 2020, arXiv:2005.11208
Bentz, M. C., Walsh, J. L., Barth, A. J., et al. 2009, ApJ, 705, 199
Blandford, R. D., & Payne, D. G. 1982, MNRAS, 199, 883
Blandford, R. D., & Znajek, R. L. 1977, MNRAS, 179, 433
Boroson, T. A., & Green, R. F. 1992, ApJS, 80, 109
Böttcher, M., & Dermer, C. D. 2002, ApJ, 564, 86
Cao, X., & Jiang, D. R. 1999, MNRAS, 307, 802
Cardelli, J. A., Clayton, G. C., & Mathis, J. S. 1989, ApJ, 345, 245
Celotti, A., & Ghisellini, G. 2008, MNRAS, 385, 283
Celotti, A., Padovani, P., & Ghisellini, G. 1997, MNRAS, 286, 415
Chai, B., Cao, X., & Gu, M. 2012, ApJ, 759, 114
Chen, L. 2018, ApJS, 235, 39
Chen, Y., Gu, Q., Fan, J., et al. 2021, ApJ, 913, 93
Cheng, K. S., Fan, J. H., & Zhang, L. 1999, A&A, 352, 32
Cohen, R. D., Rudy, R. J., Puetter, R. C., Ake, T. B., & Foltz, C. B. 1986, ApJ, 311, 135
Fan, J. H. 2005, A&A, 436, 799
Fan, J.-H., Bastieri, D., Yang, J.-H., et al. 2014, RAA, 14, 1135
Fan, J. H., Cheng, K. S., Zhang, L., & Liu, C. H. 1997, A&A, 327, 947
Fan, J.-H., Huang, Y., He, T.-M., et al. 2009, PASJ, 61, 639

Fan, J. H., Kurtanidze, S. O., Liu, Y., et al. 2021, ApJS, 253, 10
Fan, J. H., Xie, G. Z., & Bacon, R. 1999, A&AS, 136, 13
Fan, J.-H., Yang, J.-H., Liu, Y., & Zhang, J.-Y. 2013, RAA, 13, 259
Fan, J. H., Yang, J. H., Liu, Y., et al. 2016, ApJS, 226, 20
Fan, J. H., Yang, J. H., Xiao, H. B., et al. 2017, ApJL, 835, L38
Feigelson, E. D., & Babu, G. J. 1992, ApJ, 397, 55
Foschini, L., Lister, M. L., Antón, S., et al. 2021, Univ, 7, 372
Fossati, G., Maraschi, L., Celotti, A., Comastri, A., & Ghisellini, G. 1998, MNRAS, 299, 433
Francis, P. J., Hewett, P. C., Foltz, C. B., et al. 1991, ApJ, 373, 465
Fu, Y. 2021, QSOFITMORE: a python package for fitting UV-optical spectra of quasars, v1.1.0, Zenodo, doi:10.5281/zenodo.5810042
Gezari, S., Hung, T., Cenko, S. B., et al. 2017, ApJ, 835, 144
Ghisellini, G., Celotti, A., Fossati, G., Maraschi, L., & Comastri, A. 1998, MNRAS, 301, 451
Ghisellini, G., Padovani, P., Celotti, A., & Maraschi, L. 1993, ApJ, 407, 65
Ghisellini, G., Tavecchio, F., Foschini, L., et al. 2010, MNRAS, 402, 497
Ghisellini, G., Tavecchio, F., Maraschi, L., Celotti, A., & Sbarrato, T. 2014, Natur, 515, 376
Guo, H., Shen, Y., & Wang, S. 2018, PyQSOFit: Python code to fit the spectrum of quasars, Astrophysics Source Code Library, ascl:1809.008
Kang, S.-J., Fan, J.-H., Mao, W., et al. 2019, ApJ, 872, 189
Kaspi, S., Maoz, D., Netzer, H., et al. 2005, ApJ, 629, 61
Kaspi, S., Smith, P. S., Netzer, H., et al. 2000, ApJ, 533, 631
Komatsu, E., Smith, K. M., Dunkley, J., et al. 2011, ApJS, 192, 18
Kovačević, M., Chiaro, G., Cutini, S., & Tosti, G. 2019, MNRAS, 490, 4770
Kovalev, Y. Y., Aller, H. D., Aller, M. F., et al. 2009, ApJL, 696, L17
Lähteenmäki, A., & Valtaoja, E. 1999, ApJ, 521, 493
LaMassa, S. M., Cales, S., Moran, E. C., et al. 2015, ApJ, 800, 144
Lin, C., Fan, J.-H., & Xiao, H.-B. 2017, RAA, 17, 066
Liodakis, I., Hovatta, T., Huppenkothen, D., et al. 2018, ApJ, 866, 137
Liodakis, I., Marchili, N., Angelakis, E., et al. 2017, MNRAS, 466, 4625
Liu, Y., Jiang, D. R., & Gu, M. F. 2006, ApJ, 637, 669
MacLeod, C. L., Ross, N. P., Lawrence, A., et al. 2016, MNRAS, 457, 389
Mao, P., Urry, C. M., Massaro, F., et al. 2016, ApJS, 224, 26
Maraschi, L., & Tavecchio, F. 2003, ApJ, 593, 667
Mattox, J. R., Bertsch, D. L., Chiang, J., et al. 1993, ApJ, 410, 609
McElroy, R. E., Husemann, B., Croom, S. M., et al. 2016, A&A, 593, L8
Moore, R. L., & Stockman, H. S. 1981, ApJ, 243, 60
Nieppola, E., Tornikoski, M., & Valtaoja, E. 2006, A&A, 445, 441
Padovani, P., & Urry, C. M. 1990, ApJ, 356, 75
Paliya, V. S., Domínguez, A., Ajello, M., Olmo-García, A., & Hartmann, D. 2021, ApJS, 253, 46
Pei, Z., Fan, J., Yang, J., Huang, D., & Li, Z. 2022, ApJ, 925, 97
Peña-Herazo, H. A., Massaro, F., Gu, M., et al. 2021, AJ, 161, 196
Punsly, B., & Tingay, S. J. 2006, ApJL, 640, L21
Romero, G. E., Cellone, S. A., & Combi, J. A. 2000, A&A, 360, L47
Sbarrato, T., Ghisellini, G., Maraschi, L., & Colpi, M. 2012, MNRAS, 421, 1764
Schlegel, D. J., Finkbeiner, D. P., & Davis, M. 1998, ApJ, 500, 525
Shaw, M. S., Romani, R. W., Cotter, G., et al. 2012, ApJ, 748, 49
Shen, Y., Hall, P. B., Horne, K., et al. 2019, ApJS, 241, 34
Shen, Y., Richards, G. T., Strauss, M. A., et al. 2011, ApJS, 194, 45
Sheng, Z., Wang, T., Jiang, N., et al. 2020, ApJ, 889, 46
Urry, C. M., & Padovani, P. 1995, PASP, 107, 803
Vestergaard, M., & Wilkes, B. J. 2001, ApJS, 134, 1
von Montigny, C., Bertsch, D. L., Chiang, J., et al. 1995, ApJ, 440, 525
Wang, J.-M., Luo, B., & Ho, L. C. 2004, ApJL, 615, L9
Wills, B. J., Wills, D., Breger, M., Antonucci, R. R. J., & Barvainis, R. 1992, ApJ, 398, 454
Xiao, H., Fan, J., Ouyang, Z., et al. 2022a, ApJ, 936, 146
Xiao, H., Ouyang, Z., Zhang, L., et al. 2022b, ApJ, 925, 40
Xiao, H., Zhu, J., Fu, L., Zhang, S., & Fan, J. 2022c, PASJ, 74, 239
Xiao, H. B., Zhu, J. T., Fan, J. H., et al. 2022d, MNRAS, 517, 4202
Xiao, P.-y., Xie, R.-F., Zeng, X.-T., et al. 2023, ApJ, 956, 48
Xie, G. Z., Liu, H. T., Cha, G. W., et al. 2005, AJ, 130, 2506
Xiong, D. R., & Zhang, X. 2014, MNRAS, 441, 3375
Xu, Y., Huang, W., Deng, H., Mei, Y., & Wang, F. 2020, ApJ, 895, 133
Yang, J., Fan, J., Liu, Y., et al. 2023, SCPMA, 66, 249511
Yang, J. H., Fan, J. H., Liu, Y., et al. 2022a, ApJS, 262, 18
Yang, W. X., Wang, H. G., Liu, Y., et al. 2022b, ApJ, 925, 120
Ye, X.-H., & Fan, J.-H. 2021, PASJ, 73, 775
Yip, C. W., Connolly, A. J., Szalay, A. S., et al. 2004a, AJ, 128, 585
Yip, C. W., Connolly, A. J., Vanden Berk, D. E., et al. 2004b, AJ, 128, 2603
Zhang, L., Chen, S., Xiao, H., Cai, J., & Fan, J. 2020, ApJ, 897, 10
Zhang, L., Liu, Y., & Fan, J. 2022, ApJ, 935, 4
Zhang, L., Yang, J., Liu, Y., & Fan, J. 2023, SCPMA, 66, 109511
Zheng, Y. G., Kang, S. J., & Li, J. 2014, MNRAS, 442, 3166
Zheng, Y. G., & Zhang, L. 2011, ApJ, 728, 105
Zhu, J. T., Lin, C., Xiao, H. B., et al. 2023, ApJ, 950, 123
Zhu, K. R., Kang, S. J., Zhou, R. X., & Zheng, Y. G. 2021, ApJ, 916, 93